Agricultural and Forest Meteorology 157 (2012) 106–115

Contents lists available at SciVerse ScienceDirect

Agricultural and Forest Meteorology

journal homepage: www.elsevier.com/locate/agrformet

Energy and surface moisture seasonally limit evaporation and sublimation from snow-free alpine tundra

John F. Knowles[a,b,*], Peter D. Blanken[a], Mark W. Williams[a,b], Kurt M. Chowanski[c]

[a] Department of Geography, University of Colorado, UCB 260, Boulder, CO 80309-0260, United States
[b] Institute of Arctic and Alpine Research, University of Colorado, UCB 450, Boulder, CO 80309-0450, United States
[c] Institute of Atmospheric Sciences, South Dakota School of Mines and Technology, 501 East Saint Joseph Street, Rapid City, SD 57701, United States

ARTICLE INFO

Article history:
Received 19 May 2011
Received in revised form 10 January 2012
Accepted 30 January 2012

Keywords:
Alpine tundra
Eddy covariance
Energy balance
Evaporation
Sublimation
Penman–Monteith equation

ABSTRACT

This study highlights the importance of landscape position and resultant snow accumulation to the hydrologic balance of snow-free alpine tundra, and suggests that modeling studies must account for seasonally dissimilar partitioning of the energy balance in order to accurately predict evaporation and/or sublimation. The eddy covariance method was used to measure the surface energy balance above high-elevation (3502 m above sea level) alpine tundra at Niwot Ridge, CO, over 3 years from 2007 to 2009. During the winter the site was characterized by wind scour, with little snow accumulation. Two co-located towers afforded the opportunity to constrain the influence of complex mountain topography on measurement uncertainty, and overall errors were comparable to other FLUXNET sites. Random measurement uncertainty for the turbulent fluxes was approximately 10% of midday summertime values. The 0.5-h mean energy balance closure was 81% over the entire measurement period, and improved to 91% during the summer when the magnitude of the turbulent fluxes was larger. In spite of 955 mm mean annual precipitation, the 24-h mean evaporative fraction was 0.39, typical of dry grassland or rangeland ecosystems. These low values were attributed to rapid, efficient removal of snow by prevailing windy conditions throughout the winter. During the summer when rainfall provided moisture, evaporation was principally limited by available energy. Overall, an average of 39% of annual precipitation was evaporated or sublimated back to the atmosphere. We conclude that the annual distribution of precipitation is an essential control on evaporation and sublimation from this ecosystem.

1. Introduction

Atmospheric water vapor accounts for about 60% of the natural greenhouse effect (IPCC, 2007), and provides the largest positive feedback in climate change model projections (Held and Soden, 2000). A robust understanding of surface–atmosphere energy and water exchange is therefore essential to predict the consequences of forecasted climate change on terrestrial ecosystems (Harding et al., 2001; Heimann and Reichstein, 2008). The latent heat flux (λE) links hydrological, meteorological, and ecological dynamics in the environment, as it describes the surface–atmosphere exchange processes of transpiration, evaporation, and sublimation (Troen and Mahrt, 1986; Oke, 1987; Kelliher et al., 1995). In alpine areas, the magnitude of these exchange processes influences water availability and quality to flora and fauna, as well as agricultural, industrial, and residential consumers downstream (Ives et al., 1997; Beniston et al., 1997). Accordingly, perturbation to the alpine hydrologic cycle has major implications for species distribution, treeline location, and water resources (Marr, 1977; Vorosmarty et al., 2000; Litaor et al., 2008).

Alpine ecosystems are among the most sensitive and vulnerable to climate change because observed air temperature (T_a) increases are particularly large (IPCC, 2007; Rebetez and Reinhard, 2008), and many high-elevation flora and fauna species already exist near the edge of their physiological temperature tolerance (Williams et al., 1998b; Körner, 1999; Walther et al., 2002). As a result, alpine tundra represents a unique early warning indicator of global environmental change (Williams et al., 2002). Relatively few studies, however, have considered alpine energy and water exchange due to the inherently remote nature, rugged terrain, and diverse microclimates that have made ecosystem-level generalizations difficult (Billings, 1973; Greenland, 1991; Seastedt et al., 2004). Short-duration studies have demonstrated the significance of evapotranspiration and sublimation to the alpine water cycle using near-surface atmospheric profiles or Bowen ratio techniques (Ledrew and Weller, 1978; Bowers and Bailey, 1989; Isard and

* Corresponding author at: Department of Geography, University of Colorado, UCB 260, Boulder, CO 80309-0260, United States. Tel.: +1 303 492 2631; fax: +1 303 492 7501.
E-mail address: John.Knowles@Colorado.edu (J.F. Knowles).

0168-1923/$ – see front matter © 2012 Elsevier B.V. All rights reserved.
doi:10.1016/j.agrformet.2012.01.017

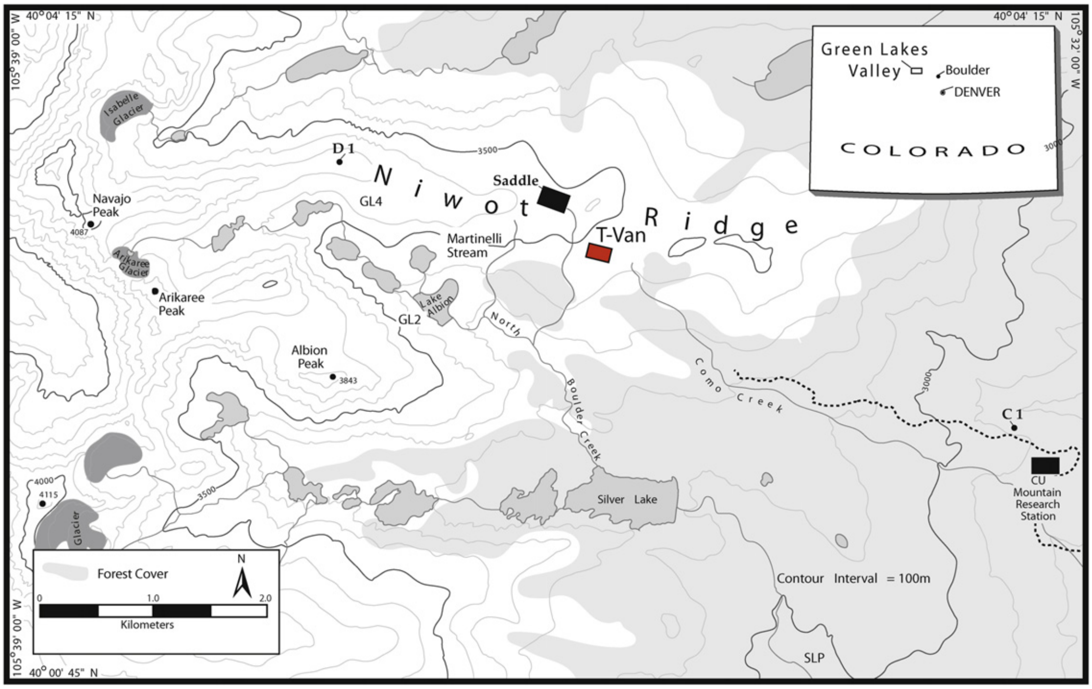

Fig. 1. T-Van is located at 3480 m asl above treeline, approximately 421 m Southeast of the Saddle research site on Niwot Ridge, CO.

Belding, 1989; Greenland, 1991; Cline, 1997; Saunders et al., 1997; Hood et al., 1999), yet continuous, robust, multi-year water loss observations from alpine tundra are still lacking. To expand the spatio-temporal scope of alpine hydrologic and energy processes, we used the eddy covariance (EC) method to continuously monitor the turbulent fluxes of water vapor exchange from alpine tundra over the course of 3 years.

Alpine tundra covers more land area (1.1×10^7 km^2; see Archibold, 1995) than any ecosystem not currently represented in the global network of long-term EC measurement sites (FLUXNET), yet remains excluded due to the difficulties associated with turbulent flux data collection in mountainous environments (Marcolla et al., 2005; Sun et al., 2007; Yi et al., 2008). Recent investigations conducted at high altitude and/or over complex terrain show the promising result, however, that EC is capable of making reasonably accurate measurements of turbulent fluxes at these locations under suitable meteorological conditions (e.g. Gu et al., 2008; Leuning et al., 2008; Blanken et al., 2009). Our goals were to: (1) establish a continuous, long-term dataset of EC measurements over high-elevation alpine tundra within the context of a rigorous measurement uncertainty assessment, and (2) identify the intra- and inter-annual magnitude and the controls of the variability of evaporation and sublimation (λE). This information will help to conceptually and empirically model the links between meteorology and λE, in order to constrain the ecological impacts of forecasted climate change.

2. Methods

2.1. Study site

The study site was located in alpine tundra near "T-Van" (40°03′11″N; 105°35′11″W; 3480 m above sea level) on Niwot Ridge, along the Front Range of the Colorado Rocky Mountains, USA (Fig. 1). Niwot Ridge is a prominent, gently (<10°) sloping, East–West oriented interfluve, originating from the Continental Divide and extending 10–12 km in length. Bedrock for the Eastern portion of Niwot Ridge was comprised mainly of gneiss with some quartz monzonite (Komarkova and Webber, 1978). The tundra soils were moderately acidic (pH 4.5–5.5) Inceptisols with Cryochrepts (less organic matter) and Cryumbrepts (more organic matter; Burns, 1980; Fisk, 1995). Continuous climate data collection was established at the Saddle research site (Humphries et al., 2008; Litaor et al., 2008) in 1981, and remains ongoing as part of the Niwot Ridge Long Term Ecological Research (LTER) Project. The long-term T_a (1981–2008) and precipitation (P; 1982–2008) values at the Saddle site were −2.2 °C (one standard deviation (σ) = 0.1 °C), and 884 mm (σ = 215 mm), respectively. Additionally, weekly snowpits were sampled at the Saddle site as part of the LTER project. Snowpack measurements include snow depth, density, temperature, and stratigraphy (Williams et al., 1999).

Vegetation is typical of fellfield communities; slow-growing, small-statured plants occurring on the ridge crests and particularly windblown slopes, with important species based on abundance including *Carex rupestris* (curly sedge), *Paronychia pulvinata* (Rocky Mountain nailwort), *Minuartia obtusiloba* (alpine sandwort), *Trifolium dasyphyllum* (alpine clover), *Eritrichium aretioides* (arctic alpine forget-me-not), and *Silene acaulis* (moss campion; Walker et al., 2001). Leaf area index was 0.87 m^2 m^{-2}, measured as the average of percent vegetated cover at 7 fellfield plots (Niwot LTER, unpublished data). The Rocky Mountains at this location represent a barrier to the prevailing mid-latitude westerly winds (Barry and Chorley, 2003), and the resulting orographic effects include a pronounced rain shadow and powerful downsloping winds through the fall, winter and spring, but to a lesser extent during summer. These winds can scour snow completely and rapidly from exposed areas on windward slopes, and deposit large amounts of snow on leeward slopes, making snow accumulation, and water availability, highly variable on both micro- and meso-scales (Erickson et al., 2005). A spring P maximum is the result of cyclonic, easterly flow that develops along the Eastern slope of the Continental Divide, while summer P events are produced by convective storms (Greenland, 1989).

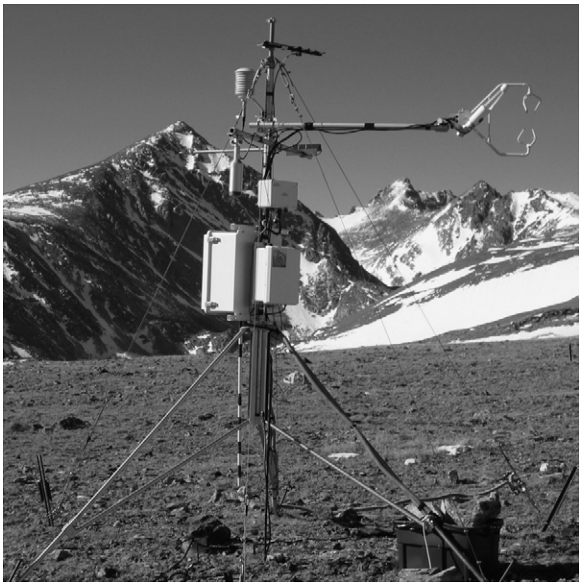

Fig. 2. Photograph of the West instrument tower on 3 February 2009 demonstrates the configuration of sensors including the CSAT 3, LI-7500, HMP 45C, and NR-Lite. Bare ground is characteristic of the study site during the winter due to windy conditions that prevent snow accumulation.

2.2. Instrumentation

Two 3.5-m-tall micrometeorological towers were installed between February and June, 2007, with the start of simultaneous data collection on 8 June 2007. The east tower (3502 m asl) was situated 50 m Northwest of two small vans (source of 120-V AC power), and the west tower (3504 m asl) 50 m West of the East tower, aligned along the prevailing wind direction to account for possible advective air flows. Instrumentation on each tower (Fig. 2) included a three-dimensional sonic anemometer (CSAT 3, Campbell Scientific), open-path infrared gas analyzer (LI-7500, LI-COR), and humidity and air temperature sensor (shielded HMP 45C, Vaisala), all facing north. The net radiation (R_n) was measured with a net radiometer (NR-Lite, Kipp and Zonen) facing south. The measurement height (z) for all atmospheric data was 3 m above ground.

A pair of soil heat flux plates (HFT3, Radiation Energy Balance Systems) were buried 2 cm beneath the surface at each location, and soil heat flux (G) was calculated as the average of the two plates; one beneath a bare rock surface, and one beneath a vegetated soil surface in order to capture spatial heterogeneity. Volumetric soil moisture (θ) at a depth of 20 cm was measured beginning 1 January 2009 using a capacitance probe (EnviroSmart, Sentek) located 1 m Northwest of the West instrument tower. During the winter, the site was visited approximately weekly by LTER field technicians and snow depth was estimated at each visit. The P was measured at the Saddle site (approximately 420 m horizontal and 35 m vertical separation) using a precipitation gauge (5-780, Belfort) with improvised windscreen at 1 m height. Here we assume that the incoming P was similar between the Saddle site and T-Van. The P charts were manually retrieved by LTER field staff on a weekly basis, and corrected to account for P overcatch due to blowing snow (Williams et al., 1998a). Half-hour means of data sampled at 10 Hz (CSAT 3 and LI-7500), 5 s (HMP 45C; NR-Lite; HFT3), and 5 min (EnviroSmart) were calculated by a datalogger (CR 3000, Campbell Scientific), and all raw data were transmitted via radio (900 MHz Spread Spectrum, FreeWave) for archival at the Institute of Arctic and Alpine Research. Standard corrections to the flux data including the Webb adjustment (Webb et al., 1980) and two-dimensional coordinate rotation (Baldocchi et al., 1988) were performed during post-processing to account for systematic errors. Previously at this site, a correction for additional sensible heat flux (H) from heating of the open-path gas analyzer (Burba et al., 2008) was found to have a minimal effect on fluxes and was not employed (Blanken et al., 2009).

2.3. Turbulent flux data quality

An inverse Gaussian plume footprint calculation was used to quantify the upwind distance contributing to measured turbulent fluxes (Schuepp et al., 1990):

$$\frac{1}{Q}\frac{dQ}{dx} = \frac{w(z-d)}{u_* k x^2} e^{-w(z-d)/k u_* x} \tag{1}$$

where Q is the area flux density, d is the zero displacement height, k is the von Karman constant (0.41), w the vertical windspeed, and x the upwind horizontal distance from the measurement location. The combination of short vegetation, low z, and high horizontal wind speeds (U) implies that measurement synchronicity between high frequency sensors is important (Massman, 2000), however, cross-correlation analyses showed measurement synchronicity to be unaffected by deterministic errors resulting from strong U.

Random measurement uncertainty of all turbulent fluxes was calculated following both a paired measurement and successive days approach (Hollinger and Richardson, 2005). The paired measurement method uses flux measurements from each tower made under near identical conditions (independent of time) and subsequently estimates the random measurement uncertainty as the standard deviation of the difference:

$$\sigma(\delta q) = \frac{1}{\sqrt{2}}\sigma(X_1 - X_2) \tag{2}$$

where δq is the measurement uncertainty, and X_1 and X_2 represent the between-tower simultaneous measurement pair. Alternatively, Eq. (2) can be applied to fluxes collected at one location on successive days as an analog to simultaneous measurements, provided that measurement pairs are made under "equivalent" meteorological conditions to minimize the effects of non-stationarity. Hereafter, valid measurement pairs occurred when 0.5-h mean between-tower T_a, U, and R_n agreed within 3 °C, 1 m s^{-1}, and 75 W m^{-2}, respectively (equivalent to Hollinger and Richardson (2005) excepting substitution of R_n for their use of 0.5-h photosynthetic photon flux density within 75 μmol m^{-2} s^{-1}).

Double-exponential (Laplace) probability distribution functions (PDFs) were also generated to characterize random uncertainty of turbulent fluxes given that previous studies have shown PDFs of random flux measurement uncertainty are most accurately described in this way (e.g. Richardson et al., 2006; Alfieri et al., 2011):

$$f(x) = \frac{e^{-|x/\beta|}}{2\beta} \tag{3}$$

where

$$\beta = \frac{\sum_{i=1}^{N}|x_i - \bar{x}|}{N} \tag{4}$$

and N is equal to sample size and x is a discrete measurement. Normal PDF analyses were also calculated (see Rogerson, 2006):

$$f(x) = \frac{1}{\sigma\sqrt{2\pi}} e^{-(x-\bar{x})^2/2\sigma^2} \tag{5}$$

Both normal and double-exponential PDFs were multiplied by the bin size of the corresponding differenced-measurement histogram to normalize to the actual data.

Surface energy balance closure was determined as the slope of the best-fit line resulting from ordinary least squares linear regression of the independent variable ($R_n - G$) against the dependent variable ($\lambda E + H$). Although the magnitude of turbulent fluxes was never significantly different between the East and West tower, a 3-year data set spanning the period 8 June 2007 through 7 June 2010, and containing equal number datapoints from each tower, was used for all qualitative and quantitative analyses unless otherwise specified.

The bulk canopy conductance (g_c) was calculated using a rearranged form of the Penman–Monteith combination equation (see Blanken, 2002):

$$\frac{1}{g_c} = r_c = \frac{r_a[S(R_n - G) - \lambda E(S + \gamma)] + \rho C_p D}{\gamma \lambda E} \quad (6)$$

where r_c is the bulk canopy resistance, S is the rate of increase of saturation vapor pressure with T_a, γ is the psychrometric constant ($\rho C_p/\lambda E$), ρ and C_p are the density and specific heat of air at constant pressure, and the aerodynamic resistance (r_a) is equal to the sum of the canopy boundary layer (r_b) and eddy diffusive (r_e) resistances, respectively (Blanken and Black, 2004):

$$r_a = \frac{B^{-1}}{u_*} + \frac{U}{u_*^2} \quad (7)$$

such that B^{-1} is the dimensionless sublayer Stanton number (2.75) and u_* is friction velocity.

The Penman–Monteith equation was also used to separate the available energy and advective influences on λE (McNaughton and Jarvis, 1983):

$$\lambda E = \frac{S}{(S + \gamma)}(R_n - G) + \frac{\rho C_p[D - D_{eq}]}{(S + \gamma)r_a + \gamma r_c} \quad (8)$$

where the equilibrium saturation deficit (D_{eq}) is given by

$$D_{eq} = \frac{S}{(S + \gamma)} \frac{\gamma r_c}{\rho C_p}(R_n - G) \quad (9)$$

such that terms to the left of the addition sign dictate the limits on λE imposed locally by $R_n - G$, while those to the right correspond to regionally imposed values of D, r_c, and r_a.

3. Results and discussion

Seasonal patterns were observed between T_a, U, and vapor pressure deficit (D). Specifically, high U and low T_a and D characterized the site during the winter, whereas decreased U, but increased T_a and D, were typical over the summer (Fig. 3). The mean annual T_a, U, and D were −1.3 °C, 8.8 m s^{-1}, and 0.3 kPa, respectively, while median wind direction was 270°. Mean annual total 2007–2009 P was 955 mm with a minimum of 831 mm (2007) and maximum of 1119 mm (2008). Maximum 0.5-h mean T_a during the study period was 19.5 °C on 31 July 2008, and minimum T_a was −27.0 °C on 15 January 2008. Peak 0.5-h mean U was 40.1 m s^{-1} on 7 January 2009, and 10-day mean U commonly reached 15 m s^{-1} in the winter.

Previous research at T-Van demonstrated that blowing snow occurs on 50% of winter days and 95% of January days, with an average of 31 blowing snow events occurring annually (mean event duration = 35 h; Berg, 1986), limiting the formation of a seasonal snowpack at the site. Indeed, field visits confirmed that midwinter snow rarely accumulated, and higher density (more resistant to wind scour) springtime snow generally lasted only hours-to-days. The lack of a persistent erodible snow cover throughout the winter indicates that snow transport in this system was snow (not wind) limited (Tabler, 2003). Although snow (not rain) remains characteristic of the tundra throughout the spring, a physical change from less dense to more dense snow gradually occurs as a result of higher T_a (Gutmann et al., 2011), which also increases the U threshold value for saltation and suspension of snow (Pomeroy et al., 1997). We therefore attribute patterns of θ in part to the depositional difference between lower-density midwinter snow versus higher-density spring snow and rain.

Between 2009 and 2010, the mean θ was only 2.8%, and a seasonal cycle was observed despite relatively evenly distributed P throughout the year (Fig. 4A and B). The θ was decoupled from P between approximately 15 November and 15 April of each year, when there was little if any snowmelt, and infiltration did not occur to the 20-cm measurement depth. Over the remainder of the year, θ was strongly linked to P and θ peaked concurrently with P during the spring (maximum θ = 36.0% on 21 May 2009). It is likely that the soils are never saturated, and surface runoff was not observed. As such, evaporation and sublimation (discussed in Section 3.3), blowing snow transport (during winter), and subsurface water storage (as θ throughout the rest of the year) represented the principal hydrologic pathways.

3.1. Systematic and random measurement uncertainty

Turbulent flux footprints were relatively short compared to the scale of landscape heterogeneity (Fig. 1), exhibiting maximum sensitivity to upwind distances of 44, 50, and 48 m upwind during average daytime, nighttime, and neutral atmospheric stability conditions. In all, 80% of turbulent fluxes were contained within 388 to 449 m upwind. An elevation difference of 35 m occurred within this footprint, indicating a slope of 7.8%. Footprints were consistent, lengthwise and directionally, due to prevalent near-neutral stability conditions fostered by strong westerly (downsloping) winds, especially during the winter (see wind rose Blanken et al., 2009, Fig. 2). Summers were characterized by convection that decreased atmospheric stability (and the flux footprint), improving data quality.

Random error distributions were strongly leptokurtic with the magnitude of kurtosis inversely proportional to the magnitude of flux (Fig. 5). Using $2\beta^{0.5}$ over successive days, random error averaged 23 W m^{-2} for both λE and H, or about 10% of midday summertime values (Table 1), comparable to grassland, forested, and agricultural FLUXNET sites (Richardson et al., 2006). The mean difference between observed and predicted frequencies for λE and H using paired measurements was 34.6 and 21.4% for double-exponential PDFs, and 48.5 and 42.8% for normal PDFs, respectively. Differencing successive days decreased the disparity between observed and predicted λE and H to 16.1 and 18.2% for double-exponential PDFs, and 43.7 and 37.0% normal PDFs. Accordingly, double-exponential distributions were the best predictors of random error, and fluxes differenced over time were the most accurately described.

Autocorrelation from closely spaced towers has been shown to cause systematic underestimation of flux error (Rannik et al., 2006), hence our results (random errors greater over space than time) suggest spatial heterogeneity poses a particular difficulty in alpine areas. Ecological variability resulting from snow distribution is well documented in both arctic and alpine tundra (Pomeroy et al., 1997; Harding et al., 2001; Liptzin et al., 2009), and λE was always relatively greater at the east tower during short (hours-to-days) periods of snow accumulation (though annual between-tower energy fluxes were not statistically different), in spite of any noticeable difference in aspect or slope angle. To investigate, snow courses were measured weekly during the 2008–2009 winter, and snow accumulation at the East tower was approximately two times higher than at the West tower. The leftward-shifted peaks of both double-exponential and normal PDFs associated with between-tower analyses (Fig. 5A and B) are therefore attributed to this snow accumulation inequality.

The 0.5-h mean energy balance closure averaged 81%, and ranged between 91% (JJA) and 67% (DJF). Summer values compared favorably to the Tibetan alpine grassland and Niwot AmeriFlux

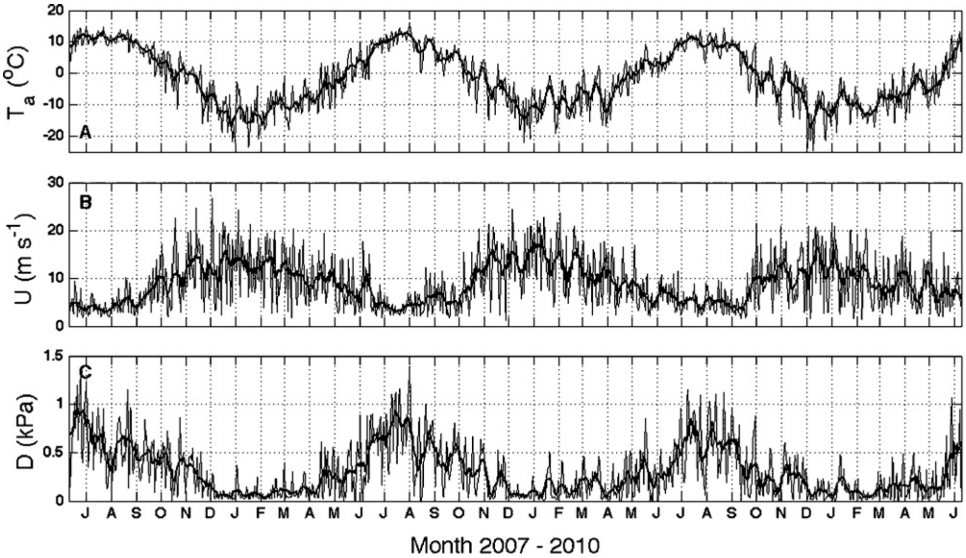

Fig. 3. The 24-h (thin line) and 10-day running (thick line) mean (A) air temperature, (B) wind speed, and (C) vapor pressure deficit between 8 June 2007 and 7 June 2010.

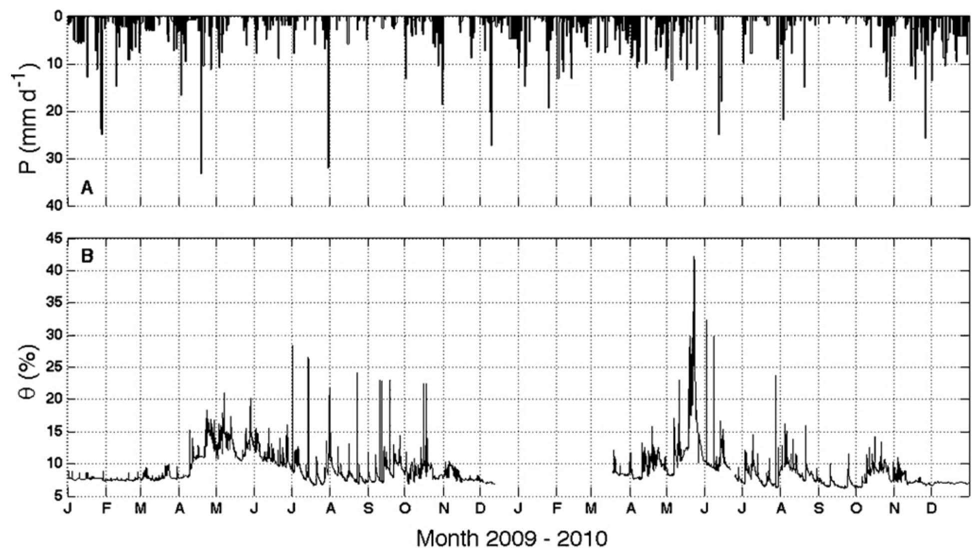

Fig. 4. (A) Daily total precipitation at the Saddle and (B) 0.5-h mean soil moisture at a depth of 20 cm between 1 January 2009 and 31 December 2010.

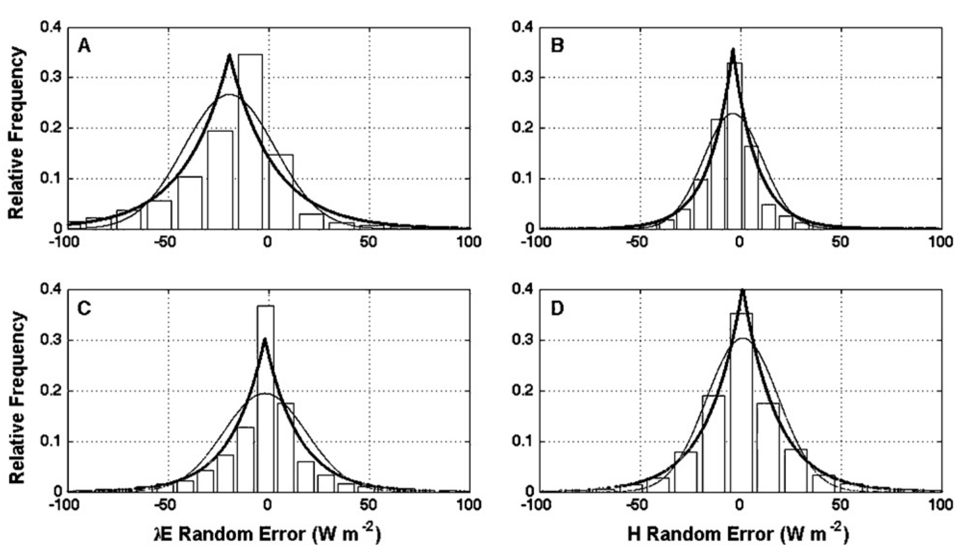

Fig. 5. Probability density functions of random measurement error determined using both (A and B) the two tower and (C and D) the successive days approaches. Thick lines represent a double-exponential distribution and thin lines the normal distribution.

Table 1
Random measurement uncertainty of 0.5-h means of λE and H for the period 8 June 2007 through 7 June 2010, including midday ($R_n > 400\,\mathrm{W\,m^{-2}}$) and nighttime ($R_n < 100\,\mathrm{W\,m^{-2}}$) conditions where n = number of observations, σ = standard deviation of the normal distribution, and $2\beta^{0.5}$ = standard deviation of the double exponential distribution.

Flux	Mean difference	n	a	Skewness	Kurtosis	$2\beta^{0.5}$
Two tower approach						
H ($\mathrm{W\,m^{-2}}$)	−3.74	24,935	20.79	2.52	58.22	16.75
$R_n > 400$	0.25	1832	32.86	1.61	8.64	31.93
$R_n < 100$	−5.34	18,416	16.32	2.30	126.69	13.12
LE ($\mathrm{W\,m^{-2}}$)	−19.44	24,935	32.01	−0.39	10.65	30.96
$R_n > 400$	−53.80	1832	39.20	0.02	3.80	43.59
$R_n < 100$	−11.95	18,416	26.47	0.04	20.36	22.82
Successive days approach						
H ($\mathrm{W\,m^{-2}}$)	1.14	3105	25.44	0.13	9.80	23.91
$R_n > 400$	1.67	204	59.15	0.57	5.66	56.83
$R_n < 100$	−1.19	2402	58.31	−0.45	5.66	58.10
LE ($\mathrm{W\,m^{-2}}$)	−1.83	3105	29.13	0.15	17.65	23.38
$R_n > 400$	2.85	204	52.32	0.08	6.74	45.73
$R_n < 100$	−2.09	2405	51.42	0.36	7.70	46.18

subalpine forest sites (70%; Gu et al., 2008, 84%; Turnipseed et al., 2002). To identify patterns, we compared u_*, an indicator of turbulent mixing, to energy balance closure during daytime, nighttime, and 24-h periods (Fig. 6A), and also to the corresponding u_* distribution during those periods (Fig. 6B). Closure was reduced from >70 to 10% when u_* decreased from 0.3 to $0.05\,\mathrm{m\,s^{-1}}$ during the night, however, excluding periods with $u_* < 0.3\,\mathrm{m\,s^{-1}}$ reduced the mean 0.5-h energy balance closure by only 1%. Daytime energy balance closure was very good, approaching unity while u_* remained below $0.5\,\mathrm{m\,s^{-1}}$, and decreasing thereafter to approximately 80% at $u_* = 1$. Energy balance closure greater than unity between $u_* = 0.2$ and $0.3\,\mathrm{m\,s^{-1}}$ remained within the measurement uncertainty range for daytime conditions (Table 1).

3.2. Magnitude, variability, and proportionality of energy fluxes

The evaporative fraction (24-h mean; EF; $\overline{\lambda E/(\lambda E + H)}$) over the entire dataset was 0.39 (σ = 0.24), typical of dry grassland, shrubland, and rangeland sites (Kurc and Small, 2004; Wang et al., 2006). In general, the H represented a larger percentage of R_n than λE, and the 24-h mean $\lambda E/R_n$ and H/R_n were 0.25 (σ = 0.22) and 0.43 (σ = 0.21), respectively. Three continuous years of R_n, H, and λE data are shown in Fig. 7A–C. The July λE (24-h mean = $63.3\,\mathrm{W\,m^{-2}}$) was slightly higher than previous estimates ($54–55\,\mathrm{W\,m^{-2}}$; Ledrew and Weller, 1978; Greenland, 1991). Compared to other ecosystems, the magnitude of G (Fig. 7D; daytime ($R_n > 0\,\mathrm{W\,m^{-2}}$) mean = $35.5\,\mathrm{W\,m^{-2}}$) was significant, owing to the lack of both vegetation and snow cover, and the relatively large fraction of exposed rock and bare soil. We also observed seasonally contrasting energy balance patterns during and immediately following P. During the winter, P generally resulted in only modest λE (Fig. 8A) as a consequence of blowing snow (Berg, 1986), reduced $R_n - G$, and lower T_a (Fig. 3). Comparable magnitude P in summer, however, produced a three-fold greater λE increase (Fig. 8B), demonstrating the importance of seasonality to the link between P and λE in this system.

3.3. Evaporation and sublimation

Between 2008 and 2010, mean annual cumulative evaporation was 399 mm (σ = 32 mm), an average of 39% (σ = 2%) of P during those years. Monthly water loss values reached a June maximum (mean = 63.3 mm, σ = 9.4 mm) and a January minimum (mean = 8.7 mm, σ = 8.5 mm). Estimates of evaporation during the month of July were 16% higher than those previously determined using near-surface profile measurements near the study

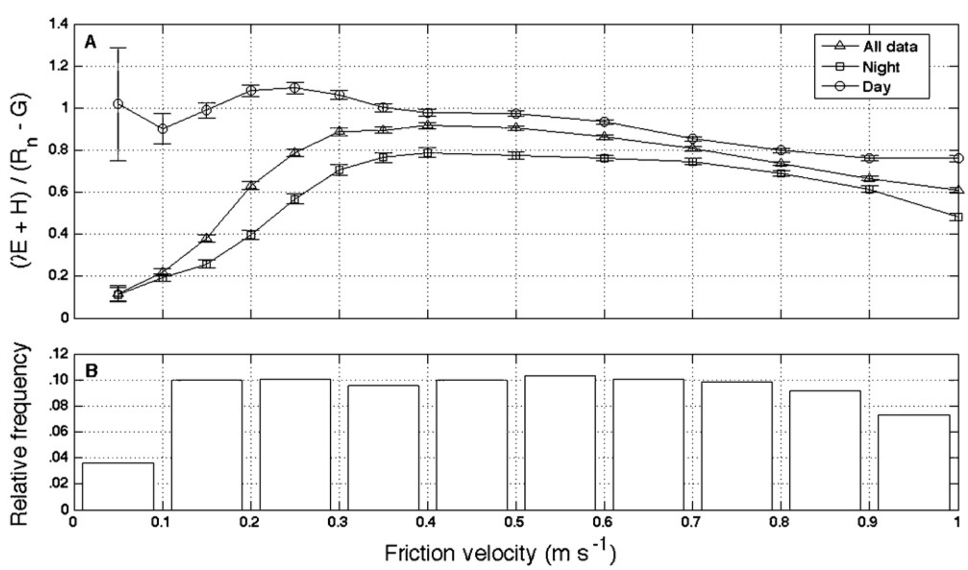

Fig. 6. (A) Energy balance closure for all 0.5-h mean data, daytime ($R_n > 30\,\mathrm{W\,m^{-2}}$), and nighttime ($R_n < -10\,\mathrm{W\,m^{-2}}$) conditions as a function of binned median friction velocity (bin size = $0.05\,\mathrm{m\,s^{-1}}$ for $u_* \le 0.4\,\mathrm{m\,s^{-1}}$ and $0.1\,\mathrm{m\,s^{-1}}$ for $u_* > 0.4\,\mathrm{m\,s^{-1}}$) during the period 8 June 2007 to 7 June 2010. Error bars are the standard error ($\sigma/n^{0.5}$ where n is the number of measurements in each bin). (B) Histogram shows the u_* distribution for all mean 0.5-h data.

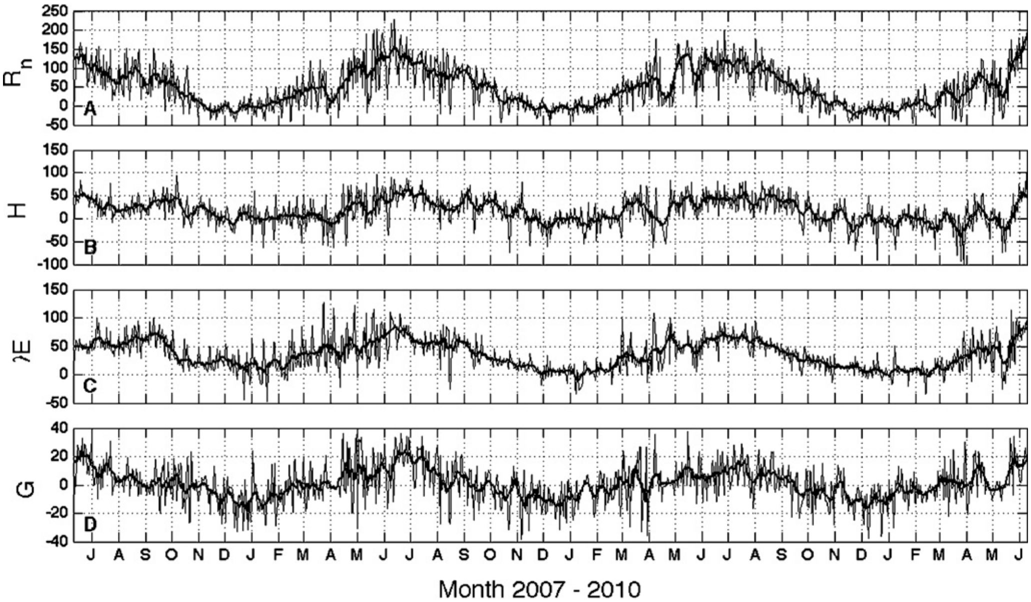

Fig. 7. Individual components of the surface energy balance in W m^{-2}. Thin lines are the 24-h mean and thick lines the 10-day running mean for (A) net radiation, (B) sensible heat flux, (C) latent heat flux, and (D) soil heat flux.

site (Ledrew and Weller, 1978; Greenland, 1991), and 116–260% higher than a survey of four arctic sites studied as part of the EU LAPP project (Lloyd et al., 2001). Two of the arctic sites, however, were underlain by permafrost, and a substantial portion of available energy was used in melting soil water in the active layer during the summer. Although $\lambda E/R_n$ was >0.5 at the two remaining (Finnish) sites, summertime P was low and limited evaporation. Excluding blowing snow, 75% of annual evaporation (298 mm; σ = 19 mm) at T-Van occurred between April and September, while just 101 mm (σ = 17 mm) was sublimated between October and March. Hereafter, these periods are classified as "summer" and "winter" unless otherwise noted.

These data contrast previous results from nearby (521 m Northwest; Subnivean Laboratory; 3537 m asl) moist tundra on Niwot Ridge, in which October through March water loss due to sublimation was 226 mm (224% greater) due to the presence of a seasonal snowpack (Hood et al., 1999). Notwithstanding, sublimation estimates associated with blowing snow that originates from T-Van are necessary in order to close the watershed-scale hydrologic balance. At high U, blowing snow is principally transported in suspension (as opposed to saltation or creep), with up to 90% of snow in suspension at U > 17 m s^{-1} (Pomeroy and Male, 1992). In general, for continental climates such as the Rocky Mountains, 57% of suspended snow will sublimate within 3 km, and 85% of suspended snow sublimates within 10 km downwind (Tabler, 2003). Therefore, given 541 mm (σ = 88 mm) average winter P, subtracting the 101 mm snow that sublimates in situ, and conservatively estimating that 75% of remaining P is transported as blowing snow in suspension, an additional 188 and 281 mm sublimation occurred within 3 and 10 km downwind, respectively. Combined with in situ

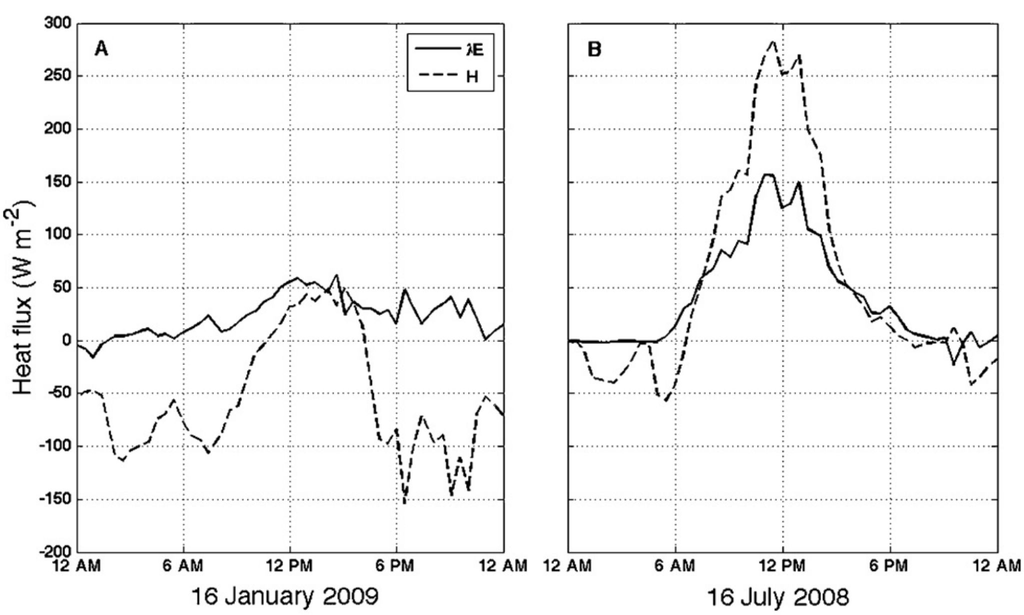

Fig. 8. Turbulent heat fluxes respond differentially to precipitation during (A) winter and (B) summer. A total of 12.9 and 11.0 mm precipitation occurred on each day. Time of day is Mountain Standard Time.

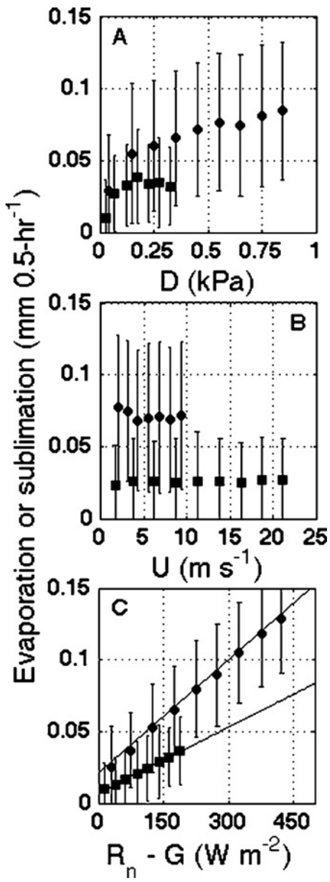

Fig. 9. Seasonal comparison of 0.5-h mean evaporation and sublimation as a function of binned daytime ($R_n > 0\,W\,m^{-2}$) meteorology. Circles are summer (April–September) data and squares are winter (October–March) data for (A) vapor pressure deficit (summer bins = 0.1 kPa; winter bins = 0.05 kPa), (B) wind speed (summer bins = 1.25 m s^{-1}; winter bins = 2.5 m s^{-1}), and (C) available energy (summer bins = 50 W m^{-2}; winter bins = 25 W m^{-2}) fit with ordinary least squares linear regression (summer and winter R^2 = 0.99). Bins containing <5% of data were omitted. Error bars are the standard deviation of the dependant variable. The standard error was <0.025 mm 0.5-h^{-1} for all binned data points.

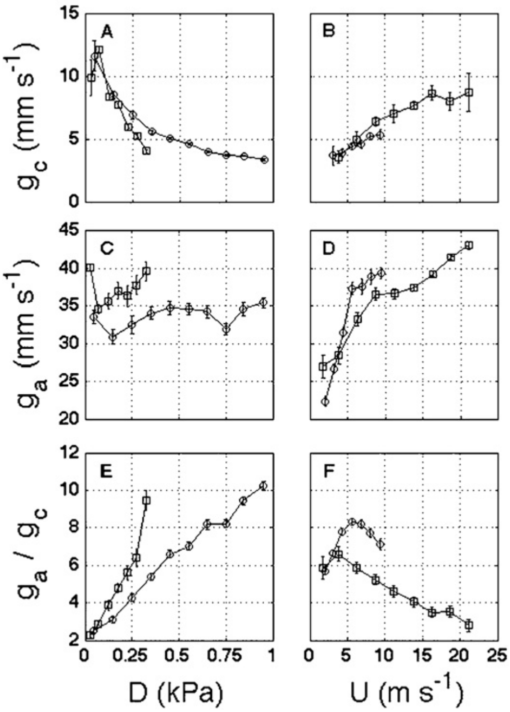

Fig. 10. Summer (circles) and winter (squares) analysis of binned 0.5-h mean vapor pressure deficit (summer bins = 0.1 kPa; winter bins = 0.05 kPa) and wind speed (summer bins = 1.25 m s^{-1}; winter bins = 2.5 m s^{-1}) versus (A and B) bulk canopy conductance, (C and D) aerodynamic conductance, and (E and F) the ratio of aerodynamic to bulk canopy conductance. Data are daytime ($R_n > 0\,W\,m^{-2}$) only. Error bars are the standard error of the dependant variable. Bins containing <5% of data were omitted.

sublimation of 101 mm, the watershed-scale cumulative annual total increased to 289–392 mm, which was equal to 97–132% of summer evaporation (298 mm), and 128–173% of comparable wintertime sublimation associated with seasonally snow-covered tundra (226 mm; Hood et al., 1999). On this larger scale, between 53 and 72% of winter P was eventually sublimated to the atmosphere. The fraction of snow that was not transported away from the site in suspension likely moved through saltation or creep into the forest adjacent to, and downwind of T-Van, where further sublimation would be expected (Molotch et al., 2007).

Future climate predictions for the Rocky Mountain region predict 50% less snowfall in winter, but 54% to 184% more summer P (Baldwin et al., 2003; Mote et al., 2005). Since T-Van was characterized locally by maximum evaporation during the summer, this translates to relatively unchanged sublimation (winter scenario; P has little effect on λE), but augmented evaporation (summer scenario; P has direct effect on λE) from snow-free alpine tundra following these results. At the watershed-scale, however, blowing snow drastically increased winter sublimation, suggesting that decreased winter snowfall would also decrease sublimation since this is a snowfall-limited process.

The seasonal correlation between D, U, $R_n - G$, and evaporation and sublimation during the day ($R_n > 0\,W\,m^{-2}$, when 85% of water loss occurred), is shown in Fig. 9. During the summer, D was relatively large (Fig. 3C) and water flux responded to D in a predictable way (Fig. 9A). The D was not correlated with sublimation during the winter, however, in part because low T_a kept the saturation vapor pressure low. Interestingly, in spite of the strong impact of U on general meteorology at this location (Blanken et al., 2009), there was no relationship between U and evaporation at any time of year (Fig. 9B). As a result, the principal impact of windy conditions seems to be the physical removal and redistribution of snow away from the study site throughout the winter. Overall, $R_n - G$ was the best predictor of both evaporation and sublimation (binned summer and winter R^2 = 0.99), though the response of water loss to increased $R_n - G$ was 89% greater in summer.

3.4. Bulk surface and aerodynamic conductance

Considering only daytime ($R_n > 0\,W\,m^{-2}$) conditions, the second term on the right-hand-side of Eq. (8) was 33% (σ = 21%) the size of the first term. This value is typically around 25% for areas of short grass with wet or dry surfaces (McNaughton and Jarvis, 1983), and so highlights a typical or even slightly greater influence of U and regional-scale air masses on λE in this system despite high $R_n - G$. Delving into that equation, an inverse relationship between D and g_c was found throughout the year (Fig. 10A), generally characteristic of plant response to increasingly dry air. Increasing U, on the other hand, slightly increased g_c (Fig. 10B), indicative of a more soil moisture-dominated g_c signal. As expected, the g_a was highest during the winter, in conjunction with the lowest D and greatest U (Fig. 10C and D). Overall, the magnitude of g_a (mean = 39 mm s^{-1}; σ = 25 mm s^{-1}) was between 2 and 10 times greater than g_c (mean = 7 mm s^{-1}; σ = 54 mm s^{-1}), and likely explains the relatively heavily weighted second term in Eq. (8). In general, the ratio of g_a to g_c was proportional to D (Fig. 10E), inversely proportional to U (Fig. 10F), and largely a function of g_c variability.

4. Conclusions

(1) We quantified both random and systematic errors of the eddy covariance method in alpine tundra. Random error calculated over successive days was approximately 10% of peak flux density for both λE and H, and was accurately described with a double-exponential PDF. Estimates of random error were significantly greater using paired measurements, due to snow accumulation and surface moisture differences between two towers spaced 50 m apart. Energy balance closure was proportional to the magnitude of flux density and u_*, but prevailing windy conditions generally kept u_* values within the range of good closure. Micro-scale ecological variability will likely present an ongoing challenge to modeling studies and meaningful application of the paired measurement approach in alpine tundra areas.

(2) The mean *EF* was typical of a dry site, and θ was particularly low throughout the winter, when windy conditions prevented snow accumulation. Overall, in situ evaporation was an order of magnitude greater during the summer relative to winter, and 75% of annual evaporation occurred between 1 April and 30 September. These findings sharply contrast previous data collected over moist alpine tundra, where in situ winter sublimation losses are critical to the hydrologic cycle. Consideration of sublimation associated with blowing snow, however, demonstrated a dominant effect of this process at the watershed-scale, and 72% of winter *P* was sublimated within 10 km downwind. Consequently, although in situ sublimation from snow-free alpine tundra is less than from snow-covered alpine tundra, the overall contribution of this process at the watershed-scale may be significantly larger due to sublimation associated with blowing snow in suspension. On this larger scale, winter sublimation was approximately equal to or greater than summer evaporation. Cumulatively, in situ evaporation and sublimation were 39% of mean annual *P*, and were strongly influenced by the seasonal distribution of *P*, because of the physically distinct deposition characteristics of dry snow, wet snow, and rain. Process-based conceptual and/or empirical models seeking to predict alpine tundra λE must take note of this seasonal disparity to accurately predict hydrologic fluxes throughout the year. Although $R_n - G$ was the best overall predictor of both evaporation and sublimation, analysis of the Penman–Monteith equation demonstrated that λE was alternately moisture- and energy-limited on a winter-to-summer basis.

Acknowledgments

The research was supported by NSF grants DEB 0423662 to the Niwot Ridge LTER program and EAR 0738780. We thank the University of Colorado Mountain Research Station staff for logistical and technical support, especially Dr. Bill Bowman, Kelly Matheson, and Guy Pfeiffer. Dr. Joe Alfieri provided useful input on an early version of this manuscript, and comments by Dr. John Gash and two anonymous reviewers greatly improved the quality of this work.

References

Alfieri, J.G., Kustas, W.P., Prueger, J.H., Hipps, L.E., Chavez, J.L., French, A.N., Evett, S.R., 2011. Intercomparison of Nine Micrometeorological Stations during the BEAREX08 Field Campaign. J. Atmos. Oceanic Technol. 28 (11), 1390–1406.
Archibold, O.W., 1995. Ecology of World Vegetation. Chapin and Hall, London.
Baldocchi, D.D., Hicks, B.B., Meyers, T.P., 1988. Measuring biosphere-atmosphere exchanges of biologically related gases with micrometeorological methods. Ecology 69 (5), 1331–1340.
Baldwin, C., Wagner, F., Lall, U., 2003. Rocky Mountain/Great Basin regional climate-change assessment report for the U.S. global change research program. In: Wagner, F. (Ed.), Water Resources. Utah State University Press, Logan, UT, pp. 79–112.
Barry, R.G., Chorley, R.J., 2003. Atmosphere, Weather, and Climate, 8th ed. Routledge Publishing, New York.
Beniston, M., Diaz, H.F., Bradley, R.S., 1997. Climatic change at high elevation sites: an overview. Clim. Change 36 (3–4), 233–251.
Berg, N.H., 1986. Blowing snow at a Colorado alpine site – measurements and implications. Arctic Alp. Res. 18 (2), 147–161.
Billings, W.D., 1973. Arctic and alpine vegetations – similarities, differences, and susceptibility to disturbance. BioScience 23 (12), 697–704.
Blanken, P.D., 2002. Canopy processes. In: Holton, J.P., Curry, J.A., Doyle, J. (Eds.), Encyclopedia of Atmospheric Sciences. Academic Press, London, pp. 1121–1130.
Blanken, P.D., Black, T.A., 2004. The canopy conductance of a boreal aspen forest, Prince Albert National Park. Can. Hydrol. Processes 18 (9), 1561–1578.
Blanken, P.D., Williams, M.W., Burns, S.P., Monson, R.K., Knowles, J., Chowanski, K., Ackerman, T., 2009. A comparison of water and carbon dioxide exchange at a windy alpine tundra and subalpine forest site near Niwot Ridge, Colorado. Biogeochemistry 95 (1), 61–76.
Bowers, J.D., Bailey, W.G., 1989. Summer energy-balance regimes for alpine tundra, Plateau Mountain, Alberta. Can. Arctic Alp. Res. 21 (2), 135–143.
Burba, G.G., McDermitt, D.K., Grelle, A., Anderson, D.J., Xu, L.K., 2008. Addressing the influence of instrument surface heat exchange on the measurements of CO_2 flux from open-path gas analyzers. Global Change Biol. 14 (8), 1854–1876.
Burns, S.F., 1980. Alpine soil distribution and development, Indian Peaks, Colorado Front Range. Ph.D. Dissertation, University of Colorado, Boulder.
Cline, D.W., 1997. Snow surface energy exchanges and snowmelt at a continental, midlatitude alpine site. Water Resour. Res. 33 (4), 689–701.
Erickson, T.A., Williams, M.W., Winstral, A., 2005. Persistence of topographic controls on the spatial distribution of snow in rugged mountain terrain, Colorado, United States. Water Resour. Res. 41 (Art. no. W04014).
Fisk, M.C., 1995. Nitrogen dynamics in an alpine landscape. Ph.D. Dissertation, University of Colorado, Boulder.
Greenland, D., 1991. Surface-energy budgets over alpine tundra in summer, Niwot Ridge, Colorado Front Range. Mt. Res. Dev. 11 (4), 339–351.
Greenland, D., 1989. The climate of Niwot Ridge, Front Range, Colorado, USA. Arctic Alp. Res. 21 (4), 380–391.
Gu, S., Tang, Y.H., Cui, X.Y., Du, M., Zhao, L., Li, Y., Xu, S.X., Zhao, H., Kato, T., Qi, P.T., Zhao, X., 2008. Characterizing evapotranspiration over a meadow ecosystem on the Qinghai-Tibetan Plateau. J. Geophys. Res. D: Atmos. 113 (Art. no. D08118).
Gutmann, E.D., Larson, K.M., Williams, M.W., Nievinski, F.G., Zavorotny, V., 2011. Snow measurement by GPS interferometric reflectometry: an evaluation at Niwot Ridge. Colorado. Hydrol. Processes, doi:10.1002/hyp.8329.
Harding, R.J., Gryning, S.E., Halldin, S., Lloyd, C.R., 2001. Progress in understanding of land surface/atmosphere exchanges at high latitudes. Theory Appl. Climatol. 70 (1–4), 5–18.
Heimann, M., Reichstein, M., 2008. Terrestrial ecosystem carbon dynamics and climate feedbacks. Nature 451 (7176), 289–292.
Held, I.M., Soden, B.J., 2000. Water vapor feedback and global warming. Annu. Rev. Energy Environ. 25, 441–475.
Hollinger, D.Y., Richardson, A.D., 2005. Uncertainty in eddy covariance measurements and its application to physiological models. Tree Physiol. 25 (7), 873–885.
Hood, E., Williams, M., Cline, D., 1999. Sublimation from a seasonal snowpack at a continental, mid-latitude alpine site. Hydrol. Processes 13 (12–13), 1781–1797.
Humphries, H.C., Bourgeron, P.S., Mujica-Crapanzano, L.R., 2008. Tree spatial patterns and environmental relationships in the forest-alpine tundra ecotone at Niwot Ridge, Colorado, USA. Ecol. Res. 23 (3), 589–605.
IPCC, 2007. In: Solomon, S., et al. (Eds.), Climate Change 2007: The Physical Science Basis. Contribution of Working Group I to the Fourth Assessment Report of the Intergovernmental Panel on Climate Change. Cambridge University Press, Cambridge/New York.
Isard, S.A., Belding, M.J., 1989. Evapotranspiration from the alpine tundra of Colorado. U.S.A. Arctic Alp. Res. 21 (1), 71–82.
Ives, J.D., Messerli, B., Speiss, E., 1997. Mountains of the world – a global priority. In: Messerli, B., Ives, J.D. (Eds.), Mountains of the World – a Global Priority. Parthenon Publishing Group, New York, pp. 1–15.
Kelliher, F.M., Leuning, R., Raupach, M.R., Schulze, E.D., 1995. Maximum conductances for evaporation from global vegetation types. Agric. For. Meteorol. 73 (1–2), 1–16.
Komarkova, V., Webber, P.J., 1978. Alpine vegetation map of Niwot ridge, Colorado. Arctic Alp. Res. 10 (1), 1–29.
Körner, C., 1999. Alpine Plant Life: Functional Plant Ecology of High Mountain Ecosystems. Springer-Verlag, Berlin.
Kurc, S.A., Small, E.E., 2004. Dynamics of evapotranspiration in semiarid grassland and shrubland ecosystems during the summer monsoon season, central New Mexico. Water Resour. Res. 40 (Art. no. W09305).
Ledrew, E.F., Weller, G., 1978. Comparison of radiation and energy-balance during growing season for an arctic and alpine tundra. Arctic Alp. Res. 10 (4), 665–678.
Leuning, R., Zegelin, S.J., Jones, K., Keith, H., Hughes, D., 2008. Measurement of horizontal and vertical advectlion of CO_2 within a forest canopy. Agric. For. Meteorol. 148 (11), 1777–1797.
Liptzin, D., Williams, M.W., Helmig, D., Seok, B., Filippa, G., Chowanski, K., Hueber, J., 2009. Process-level controls on CO_2 fluxes from a seasonally snow-covered subalpine meadow soil, Niwot Ridge, Colorado. Biogeochemistry 95 (1), 151–166.

Litaor, M.I., Williams, M., Seastedt, T.R., 2008. Topographic controls on snow distribution, soil moisture, and species diversity of herbaceous alpine vegetation, Niwot Ridge, Colorado. J. Geophys. Res. G: Biogeosci. 113 (Art. no. G02008).

Lloyd, C.R., Harding, R.J., Friborg, T., Aurela, M., 2001. Surface fluxes of heat and water vapour from sites in the European Arctic. Theory Appl. Climatol. 70 (1–4), 19–33.

Marcolla, B., Cescatti, A., Montagnani, L., Manca, G., Kerschbaumer, G., Minerbi, S., 2005. Importance of advection in the atmospheric CO_2 exchanges of an alpine forest. Agric. For. Meteorol. 130 (3–4), 193–206.

Marr, J.W., 1977. Development and movement of tree islands near upper limit of tree growth in Southern Rocky Mountains. Ecology 58 (5), 1159–1164.

Massman, W.J., 2000. A simple method for estimating frequency response corrections for eddy covariance systems. Agric. For. Meteorol. 104 (3), 185–198.

McNaughton, K.G., Jarvis, P.G., 1983. Predicting effects of vegetation changes on transpiration and evaporation. In: Kozlowski, T.T. (Ed.), Water Deficits and Plant Growth, Volume VII. Academic Press, New York.

Molotch, N.P., Blanken, P.D., WIlliams, M.W., Turnipseed, A.A., Monson, R.K., Margulis, S.A., 2007. Estimating sublimation of intercepted and sub-canopy snow using eddy covariance systems. Hydrol. Processes 21 (12), 1567–1575.

Mote, P.W., Hamlet, A.F., Clark, M.P., Lettenmaier, D.P., 2005. Declining mountain snowpack in Western North America. Bull. Am. Meteorol. Soc. 86 (1), 39–49.

Oke, T.R., 1987. Boundary Layer Climates, 2nd ed. Routledge Publishing, New York.

Pomeroy, J.W., Male, D.H., 1992. Steady-state suspension of snow. J. Hydrol. 136 (1–4), 275–301.

Pomeroy, J.W., Marsh, P., Gray, D.M., 1997. Application of a distributed blowing snow model to the arctic. Hydrol. Processes 11 (11), 1451–1464.

Rannik, U., Kolari, P., Vesala, T., Hari, P., 2006. Uncertainties in measurement and modelling of net ecosystem exchange of a forest. Agric. For. Meteorol. 138 (1–4), 244–257.

Rebetez, M., Reinhard, M., 2008. Monthly air temperature trends in Switzerland 1901–2000 and 1975–2004. Theor. Appl. Climatol. 91 (1–4), 27–34.

Richardson, A.D., Hollinger, D.Y., Burba, G.G., Davis, K.J., Flanagan, L.B., Katul, G.G., Munger, J.W., Ricciuto, D.M., Stoy, P.C., Suyker, A.E., Verma, S.B., Wofsy, S.C., 2006. A multi-site analysis of random error in tower-based measurements of carbon and energy fluxes. Agric. For. Meteorol. 136 (1–2), 1–18.

Rogerson, P.A., 2006. Statistical Methods for Geography: A Student's Guide, 2nd ed. Sage Publications, London.

Saunders, I.R., Bailey, W.G., Bowers, J.D., 1997. Evaporation regimes and evaporation modelling in an alpine tundra environment. J. Hydrol. 195 (1–4), 99–113.

Schuepp, P.H., Leclerc, M.Y., Macpherson, J.I., Desjardins, R.L., 1990. Footprint prediction of scalar fluxes from analytical solutions of the diffusion equation. Boundary-Layer Meteorol. 50 (1–4), 353–373.

Seastedt, T.R., Bowman, W.D., Caine, T.N., McKnight, D., Townsend, A., Williams, M.W., 2004. The landscape continuum: a model for high-elevation ecosystems. BioScience 54 (2), 111–121.

Sun, J.L., Burns, S.P., Delany, A.C., Oncley, S.P., Turnipseed, A.A., Stephens, B.B., Lenschow, D.H., LeMone, M.A., Monson, R.K., Anderson, D.E., 2007. CO_2 transport over complex terrain. Agric. For. Meteorol. 145 (1–2), 1–21.

Tabler, R.D., 2003. Controlling Blowing and Drifting Snow with Snow Fences and Road Design. National Cooperative Highway Research Program Transportation Research Board of the National Academies (Project 20-7(147)).

Troen, I., Mahrt, L., 1986. A simple-model of the atmospheric boundary-layer – sensitivity to surface evaporation. Boundary-Layer Meteorol. 37 (1–2), 129–148.

Turnipseed, A.A., Blanken, P.D., Anderson, D.E., Monson, R.K., 2002. Energy budget above a high-elevation subalpine forest in complex topography. Agric. For. Meteorol. 110 (3), 177–201.

Vorosmarty, C.J., Green, P., Salisbury, J., Lammers, R.B., 2000. Global water resources: vulnerability from climate change and population growth. Science 289 (5477), 284–288.

Walker, M.D., Walker, D.A., Theodose, T.A., Webber, P.J., 2001. The vegetation: hierarchical species–environment relationships. In: Bowman, W.D., Seastedt, T.R. (Eds.), Structure and Function of an Alpine Ecosystem: Niwot Ridge, Colorado. Oxford University Press, New York, pp. 99–127.

Walther, G.R., Post, E., Convey, P., Menzel, A., Parmesan, C., Beebee, T.J.C., Fromentin, J.M., Hoegh-Guldberg, O., Bairlein, F., 2002. Ecological responses to recent climate change. Nature 416 (6879), 389–395.

Wang, K.C., Li, Z.Q., Cribb, M., 2006. Estimation of evaporative fraction from a combination of day and night land surface temperatures and NDVI: a new method to determine the Priestley–Taylor parameter. Remote Sens. Environ. 102 (3–4), 293–305.

Webb, E.K., Pearman, G.I., Leuning, R., 1980. Correction of flux measurements for density effects due to heat and water-vapor transfer. Q. J. R. Meteorol. Soc. 106 (447), 85–100.

Williams, M.W., Bardsley, T., Rikkers, M., 1998a. Overestimation of snow depth and inorganic nitrogen wetfall using NADP data, Niwot Ridge, Colorado. Atmos. Environ. 32 (22), 3827–3833.

Williams, M.W., Brooks, P.D., Seastedt, T., 1998b. Nitrogen and carbon soil dynamics in response to climate change in a high-elevation ecosystem in the Rocky Mountains, USA. Arctic Alp. Res. 30 (1), 26–30.

Williams, M.W., Cline, D., Hartmann, M., Bardsley, T., 1999. Data for snowmelt model development, calibration, and verification at an alpine site, Colorado Front Range. Water Resour. Res. 35 (10), 3205–3209.

Williams, M.W., Losleben, M.V., Hamann, H.B., 2002. Alpine areas in the Colorado Front Range as monitors of climate change and ecosystem response. Geogr. Rev. 92 (2), 180–191.

Yi, C.X., Anderson, D.E., Turnipseed, A.A., Burns, S.P., Sparks, J.P., Stannard, D.I., Monson, R.K., 2008. The contribution of advective fluxes to net ecosystem exchange in a high-elevation, subalpine forest. Ecol. Appl. 18 (6), 1379–1390.